

# Single-Layer Wideband Circularly Polarized High-Efficiency Reflectarray for Satellite Communications

Long Zhang, Steven Gao, *Senior Member, IEEE*, Qi Luo, *Member, IEEE*, Wenting Li, Yejun He, *Senior Member, IEEE*, and Qingxia Li, *Member, IEEE*

**Abstract**—This paper presents a single-layer circularly polarized (CP) reflectarray which achieves large bandwidth in terms of axial ratio (AR), gain, aperture efficiency and radiation pattern. By using a novel wideband S-shaped phasing element, an offset-fed reflectarray with 20° offset beam is designed based on the element angular rotation method. Theoretical analysis is given to analyze the effect of angular rotated elements on the performance of the reflectarray, which indicates that the AR bandwidth of the reflectarray can exceed the AR bandwidth of the feed horn. Furthermore, the influence of the differential spatial phase delay is analyzed quantitatively, and the performance of S-element-based reflectarrays with different aperture sizes are investigated and discussed. To verify these concepts, a 180mm×180mm prototype with 15×15 elements is fabricated and measured. The measured results confirm that the proposed reflectarray achieves a 68.5% 3-dB AR bandwidth (7.0 GHz to 14.3 GHz) and a 47.8% 3-dB gain bandwidth (8.6 GHz to 14 GHz). Moreover, the aperture efficiency is larger than 50% in a 33% bandwidth and larger than 30% in a 64% bandwidth.

**Index Terms**—Circular polarization, element rotation method, reflectarray, satellite communications, wideband array.

## I. INTRODUCTION

PRINTED reflectarrays combine the advantages of parabolic antennas and planar phased arrays, which receive increasing interest in designing high-gain antennas. Generally, reflectarrays consist of radiating elements with preadjusted phases and an illuminating feed antenna to form a planar phase front in the farfield [1]. Although they have many advantages,

such as the significantly simplified feeding system, versatile beams, flat structure and low manufacturing cost, one major drawback of reflectarrays is their narrow bandwidth.

The narrow bandwidth of reflectarrays is mainly caused by two factors: the inherent narrow bandwidth of microstrip elements and the differential spatial phase delay caused by different path lengths from the feed to each element [2]. To improve the bandwidth of reflectarrays, several approaches were adopted, such as using stacked patches [3], subwavelength element [4], dual-frequency phase synthesis [5] and true time delay technique [6].

Designing circularly polarized (CP) reflectarray is necessary for some applications since the CP arrays possess the advantages of mitigation of multi-path fading, immunity of “Faraday rotation” and the reduction of polarization mismatching [7]. Two different ways have been introduced to design a CP reflectarray. The first one is using a linearly polarized (LP) feed to illuminate an aperture which is able to transform the incident LP wave to CP reflected wave and form a cophasal beam in the far-field [8, 9]. Another method to design a CP reflectarray is utilizing a CP feed as a primary source and the reflected wave can superpose in phase in the far-field. Various designs based on this approach were proposed, including using angular rotated elements [10, 11], variable sized elements [12] and elements with variable-length phase delay lines [13].

Considering that it is more difficult to design elements with wideband CP reflection performance and wideband CP feeds, the bandwidth enhancement of CP reflectarrays is thus more challenging than LP reflectarrays. To meet frequency coverage requirement, designing dual-frequency CP reflectarrays is attractive to some applications [14, 15]. However, for applications such as high-data-rate satellite communications, it is highly desirable to have CP reflectarrays with broad bandwidth [16]. Different approaches were utilized to improve the bandwidth of CP reflectarrays [9, 17-20]. Through using rectangular-patch phasing element with subwavelength grid spacing, a 17% 1-dB gain bandwidth and 11% 3-dB axial ratio (AR) bandwidth was obtained [17]. The bandwidth of CP reflectarray was further improved by using a dual-layer T-shaped phasing element, with a 1-dB gain bandwidth of 20% and 3-dB AR bandwidth of 28% [18]. Since the elements used

Manuscript received December 14, 2016. This work was supported by the U.K. Engineering and Physical Sciences Research Council under Grant EP/N032497/1, National Natural Science Foundation of China under Grant 61372077, Science and Technology Innovation Commission of Shenzhen under Grant ZDSYS 201507031550105, and Guangdong Provincial Science and Technology Programs under Grant 2013B090200011 and Grant 2016B090918080.

L. Zhang and Y. He are with the Shenzhen Key Lab of Antennas and Propagation and the Guangdong Engineering Research Center of Base Station Antennas and Propagation, College of Information Engineering, Shenzhen University, Shenzhen 518060, China (emails: longzhang717@163.com, heyejun@126.com).

S. Gao, Q. Luo and W. Li are with the School of Engineering and Digital Arts, University of Kent, Canterbury CT2 7NT, UK (email: s.gao@kent.ac.uk).

Q. Li is with the School of Electronic Information and Communications, Huazhong University of Science and Technology, Wuhan 430074, China.

in [17, 18] are resonant type, the CP reflectarray using these resonant phasing elements demonstrates a typically smaller than 30% bandwidth. Multi-resonance phasing elements such as the Jerusalem cross and open loop combined subwavelength element [9] and the dual-ring element [19] based CP reflectarrays achieved more than 30% 3-dB AR bandwidth. Another way to realize wide bandwidth of CP reflectarrays is using spatial time-delay units (TDUs) [20]. Although the CP reflectarray using TDUs achieved 40% 3-dB gain bandwidth and 3-dB AR bandwidth, the aperture efficiency was just around 40% and the multi-layer structure increased the fabrication complexity.

In this paper, a novel S-shaped phasing element which achieves smaller than -15dB cross polarization (cross-pol) reflection in a 2:1 bandwidth is proposed. Based on this novel broadband element, a single-layer CP reflectarray using angular rotated elements is designed, fabricated and measured. The measured results indicate that the proposed single-layer reflectarray achieves a 68.5% 3-dB AR bandwidth and a 47.8% 3-dB gain bandwidth. Moreover, the aperture efficiency (AE) is larger than 50% in a 33% bandwidth and larger than 30% in a 64% bandwidth. To the best knowledge of the authors, it is the widest bandwidth single-layer CP reflectarray developed up to now in terms of 3-dB AR and larger than 50% AE bandwidth.

The paper is organized as follows: Section II introduces the design of the novel S-shaped element for reflectarrays; Section III presents the design and analysis of the proposed CP reflectarray; Section IV presents the simulation and measurement results and comparisons with other reported wideband CP reflectarrays. The conclusion is in Section V.

## II. S-SHAPED ELEMENT FOR REFLECTARRAYS

Various elements have been designed and deployed in CP reflectarrays, such as the patches, stacked patches, crossed dipoles and their derivatives, split rings and the combination of several types of these elements. All these reported elements demonstrate bandwidths less than 50%. In this section, a novel S-shaped element for reflectarray application is presented and analyzed, which can achieve a bandwidth over 66%.

### A. Element Geometry

The geometry of the proposed S-shaped element is shown in Fig. 1. As shown in Fig. 1 (a) and (b), the proposed element is printed on the bottom layer of a Rogers RO4003C substrate with relative dielectric constant of 3.55, dissipation factor of 0.0027 and a thickness of  $t$ . A ground plane is placed below the substrate with a height of  $h$  which affects the element reflection performance substantially. The element is printed below the substrate in order to achieve better element reflection performance with an integral value of  $h$ , which facilitates the prototype fabrication. The size of the ground plane and the unit cell are  $L_f \times L_f$ . The S-shaped element is composed of two single arms with the same size shown in Fig. 1 (c). It can be seen from Fig. 1 (c) that each arm is obtained by subtracting a smaller sized ellipse with a rotating angle  $\alpha$  from a larger sized ellipse. To form a square-sized S-shaped element, the major radius of the bigger ellipse  $R_1$  is two times as large as the minor radius.

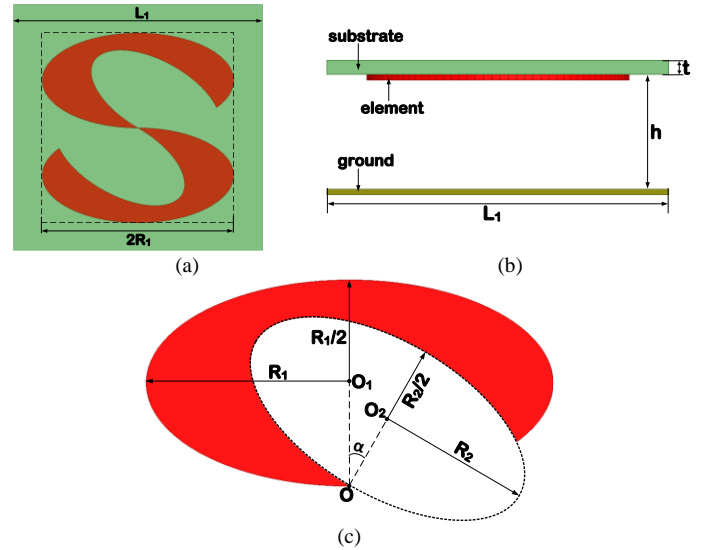


Fig. 1. Geometry of the proposed element: (a) top view, (b) side view, (c) single arm.

The proposed element is a follow-on work of the antenna presented in [21], where an inverted S-shaped antenna with wideband CP radiation was presented. However, there are significant differences between the proposed element and the antenna in [21]. The element proposed in this paper is used for reflectarray application and its reflection performance under periodical boundary environment is of major interest. The proposed phasing element has a more compact size ( $0.32\lambda \times 0.32\lambda$ ) than the antenna presented in [21] ( $0.99\lambda \times 0.42\lambda$ ). The size reduction is realized by choosing bigger rotating angle  $\alpha$  and bigger  $R_1/R_2$  ratio, which gives longer travelling-wave current path and the utilization of sub-wavelength technique. Although the size of the presented element is greatly reduced, the CP bandwidth is largely improved by 58.8% (from 42% in [21] to 66.7%). Furthermore, the proposed element can be placed in a square lattice while the antenna in [21] is only able to be placed in a rectangular lattice. The square-sized element is more advantageous to planar arrays because the rectangular-sized antenna has different electrical length along x-axis and y-axis direction, which results in uneven characteristics such as different beamwidth and AR beamwidth in the two orthogonal directions. On the contrary, the proposed element can provide relatively symmetry performance along x-axis and y-axis direction, which brings more equal mutual coupling between each elements in the two directions and thus facilitates the design and improves the performance of the reflectarray.

The detailed geometry dimensions of the proposed element are shown in Table I.

TABLE I  
ELEMENT DIMENSIONS

$L_f$	$R_1$	$R_2$	$\alpha$	$h$	$t$
12mm	4.6mm	3.45mm	30°	4mm	0.508mm

### B. Element Performance

As the electrical length of the proposed element is mainly determined by geometry parameters  $R_1$ ,  $R_2$  and rotating angle  $\alpha$ ,

the impact of these parameters to the element's performance needs to be investigated. For a brief investigation, the ratio  $R_2/R_1=0.75$  and the rotating angle  $\alpha$  is kept unchanged while only  $R_1$  is varied.

The evaluation of the element performance is conducted by using a periodic boundary and a Floquet port excitation in HFSS under normal incident plane waves. The incident field is set to be right-hand circularly polarized (RHCP). Fig. 2 shows the magnitudes of reflected RHCP field (co-pol component) and left-hand circularly polarized (LHCP) field (cross-pol component) with different  $R_1$ . As shown, the available bandwidth ( $|\Gamma_{cross-pol}| \leq -15\text{dB}$ ) of the element increases with larger  $R_1$ . As the ratio  $R_2/R_1$  is kept unchanged, this phenomenon can be explained that increasing  $R_1$  brings longer electrical length and pushes the lowest-frequency resonance to lower frequency.

As shown in Fig. 2, the element can provide a bandwidth of 2:1 (7GHz to 14GHz) within which the reflected LHCP component is smaller than -15 dB ( $|\Gamma_{cross-pol}| \leq -15\text{ dB}$ ) when  $R_1$  is 4.7 mm. Notice that  $|\Gamma_{cross-pol}|^2 + |\Gamma_{co-pol}|^2 \cong 1$  (the approximation rises from dielectric and conductor losses), thus  $|\Gamma_{cross-pol}| \leq -15\text{ dB}$  makes  $|\Gamma_{co-pol}| \geq -0.2\text{ dB}$ . To acquire lower cross-pol component reflection and adequate bandwidth simultaneously,  $R_1$  is chosen to be 4.6 mm, which achieves an available bandwidth from 7.3 GHz to 14.1 GHz and  $|\Gamma_{cross-pol}| \leq -20\text{ dB}$ ,  $|\Gamma_{co-pol}| \geq -0.1\text{ dB}$  from 7.5 GHz to 13.7 GHz.

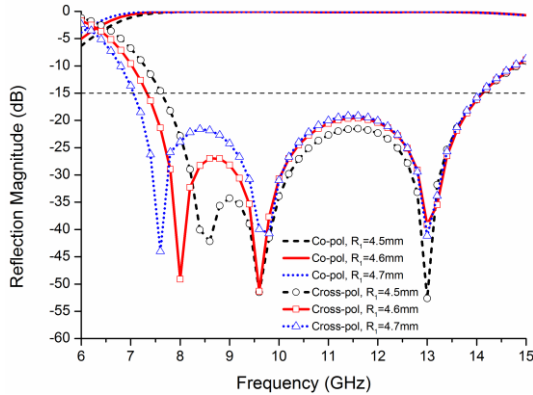


Fig. 2. The magnitude of the reflected field with different  $R_1$ .

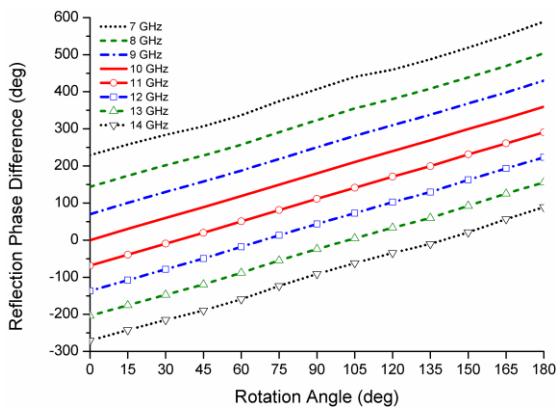


Fig. 3. The phase difference of the reflected co-pol field with different element rotation angle.

The element angular rotation method is used to provide the

desired phases for each element. It is indicated that the angular rotation angle  $\psi$  of a CP element results in a  $2\psi$  phase variation of the reflected co-pol field [10, 22]. Fig. 3 shows the phase difference of the reflected co-pol field under different element rotation angle. As shown, the element achieves a rather linear phase response to the element rotation angle  $\psi$  in a 2:1 frequency range. The phase error (actual phase difference compared with  $2\psi$ ) is smaller than  $10^\circ$  within the bandwidth.

The reflection magnitudes of the co-pol and cross-pol components with different rotation angle  $\psi$  are shown in Fig. 4. As shown, the proposed element maintains low cross-pol and good co-pol reflection in a nearly 2:1 frequency range under all rotation angles.

To give an understanding of the element reflection performance under oblique incidence, Fig. 5 gives the reflection phase of the co-pol field under different oblique incidence angle theta. As shown, the phase discrepancy of about  $7^\circ$  and  $28^\circ$  are observed for theta= $15^\circ$  and theta= $30^\circ$  incidence at the design frequency 9 GHz, respectively. It is noticed that a ripple occurs at the frequency around 8 GHz, which is assumed to be the main reason of the variation of simulated AR and gain at 8 GHz shown in Fig. 8 and Fig. 9, respectively. Besides, it is observed from simulation that the phase error is smaller than  $10^\circ$  at 9 GHz under  $30^\circ$  oblique incidence when the element is rotated, which yields not so big differences compared with the case under normal incidence. Considering that only the edge elements are illuminated at large incidence angle, thus the proposed reflectarray is designed based on the reflection phase under normal incident plane waves.

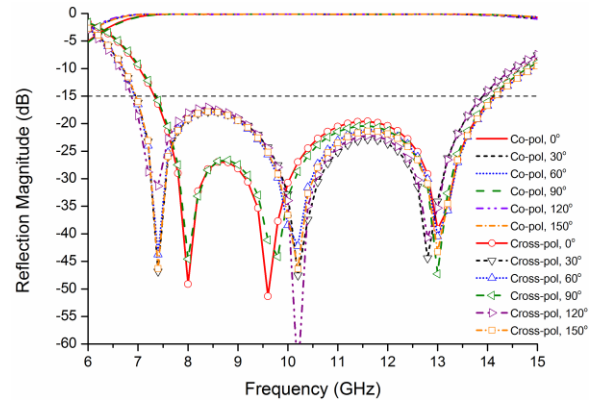


Fig. 4. The magnitude of the reflected field with different rotation angle.

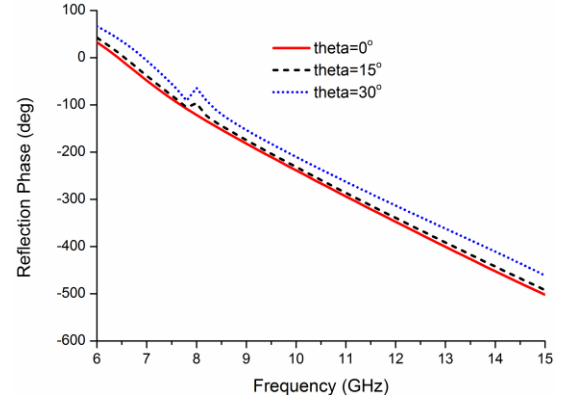


Fig. 5. Reflection phase of the co-pol field with different oblique incidence angle.

### III. REFLECTARRAY DESIGN AND ANALYSIS

In this section, the array configuration and the element phase distribution over the aperture are given. Then, the performance of the proposed reflectarray is analyzed theoretically and the conclusions are verified by using different feed horns. Finally, the effects of the differential spatial phase delay and the aperture size on the bandwidth of the proposed reflectarray are analyzed.

#### A. Array Configuration

The configuration of the proposed reflectarray is shown in Fig. 6. As shown, the reflectarray consists of 225 (15×15) S-shaped elements, each with different rotation angle to provide required phase delay. The reflectarray is designed to be fed by a wideband dual-CP horn with an offset of 20° to the Z-axis, which is aimed to minimize the blockage of the feed. It is indicated in [23] that an offset feed causes main beam scan with frequency due to a change in phase taper across the reflectarray with a change in frequency. This beam squint phenomenon can be minimized if the angle of the main beam is chosen to be close to the natural specular reflection angle. To eliminate the beam squint, the main beam direction is designed to  $\theta = -20^\circ$ . The focus-to-diameter ratio ( $f/D$ ) of 0.97 is chosen to provide an illumination with around -10dB edge tapering, which helps achieve good bandwidth performance.

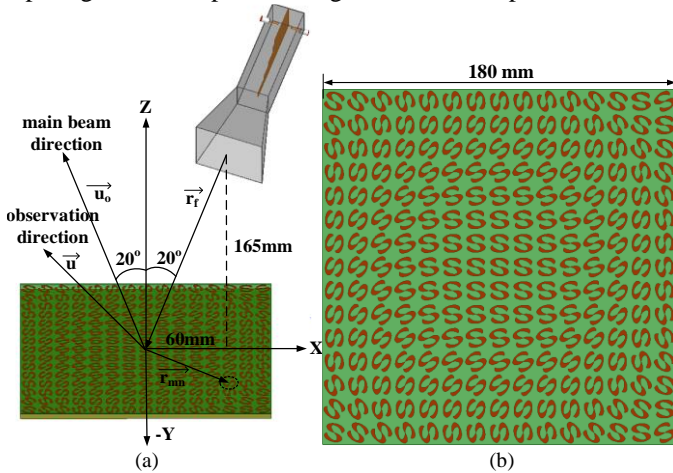


Fig. 6. Configuration of the proposed reflectarray: (a) side view, (b) top view of reflecting aperture.

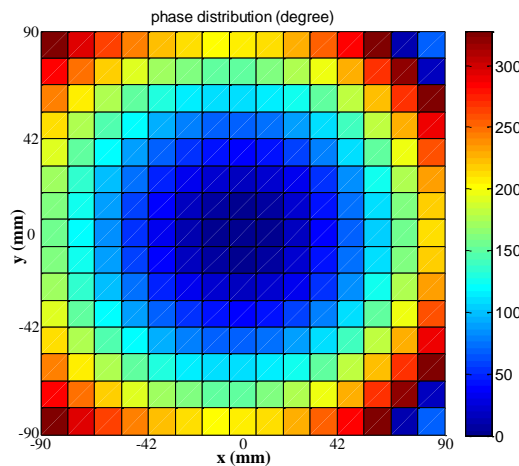


Fig. 7. Required phase distribution for each element.

The required phase distribution of each S-shaped element is shown in Fig. 7. As the element rotation angle  $\psi$  results in a  $2\psi$  phase variation of the reflected co-pol field, the phase distribution in Fig. 7 can directly map into Fig. 6 (b).

#### B. Analysis of Array Performance Using Angular Rotated Elements

It is implicit that the cross-pol of a reflectarray using element angular rotation method is degraded in the main beam region and thus the AR performance can be enhanced [10]. However, this phenomenon is not discussed in details. Besides, the reflectarray proposed in [10] is a narrow-band array, it is important to investigate whether this phenomenon still exists in a wideband reflectarray.

When a two-dimensional planar array with 15×15 elements is non-uniformly illuminated by a horn at  $r_f$ , as shown in Fig. 6 (a), the reradiated field from the array in an arbitrary direction  $\vec{u}$  can be represented by

$$E(\vec{u}) = \sum_{m=1}^{15} \sum_{n=1}^{15} F(\vec{r}_{mn} \cdot \vec{r}_f) A(\vec{r}_{mn} \cdot \vec{u}_0) A(\vec{u} \cdot \vec{u}_0) \cdot e^{-jk_0(|\vec{r}_{mn}-\vec{r}_f|+\vec{r}_{mn}\cdot\vec{u})} \cdot e^{j\phi_{mn}} \quad (1)$$

where  $F$  is the pattern function of the feed horn,  $A$  is the pattern function of the S-shaped element,  $\vec{r}_{mn}$  is the position vector of the  $m$ th element,  $\vec{u}_0$  is the desired main beam direction,  $k_0$  is the free-space wavenumber, and  $\phi_{mn}$  is the required phase delay of the  $m$ th element [10, 24].

Considering an incident wave radiated by the feed horn propagating in the  $-Z$  direction, as shown in Fig. 6 (a)

$$\vec{E}^{inc} = F_{RH}(\vec{E}_x - j\vec{E}_y)e^{jk_0z}e^{j\omega t} + F_{LH}(\vec{E}_x + j\vec{E}_y)e^{jk_0z}e^{j\omega t} \quad (2)$$

The former part represents the RHCP component of the radiated field from the horn with a magnitude of  $F_{RH}$  while the second part is the LHCP component with a magnitude of  $F_{LH}$ .

Denoting the physical counter-clockwise rotation angle of the  $m$ th element by  $\psi_{mn}$ , the reflected RHCP field by the  $m$ th S-shaped element can be written in the form

$$\vec{E}_{RHCP}^{refl} = |\Gamma_{co-pol}| \cdot F_{RH}(\vec{E}_x + j\vec{E}_y)e^{-jk_0z}e^{j\omega t} \cdot e^{-2j\psi_{mn}} + |\Gamma_{cross-pol}| \cdot F_{LH}(\vec{E}_x + j\vec{E}_y)e^{-jk_0z}e^{j\omega t} \quad (3)$$

The first part represents the reflected RHCP field from the incident RHCP component of the feed horn, and thus a counter-clockwise rotation angle  $\psi_{mn}$  of the element brings a  $-2\psi_{mn}$  phase variation to the reflected co-pol field. The second part denotes the reflected RHCP field from the incident LHCP component of the feed horn, and no additional phase variation is introduced upon reflection [10].

Similarly, the reflected LHCP field by the  $m$ th S-shaped element with rotation angle of  $\psi_{mn}$  can be represented by

$$\vec{E}_{LHCP}^{refl} = |\Gamma_{co-pol}| \cdot F_{LH}(\vec{E}_x - j\vec{E}_y)e^{-jk_0z}e^{j\omega t} \cdot e^{2j\psi_{mn}} + |\Gamma_{cross-pol}| \cdot F_{RH}(\vec{E}_x - j\vec{E}_y)e^{-jk_0z}e^{j\omega t} \quad (4)$$



It is worth pointing out that  $|\Gamma_{cross-pol}|$  used in (3) and (4) is of the same value due to reciprocity and thus is denoted by the same expression. Although the magnitudes of the reflection coefficient  $|\Gamma_{co-pol}|$  are the same in (3) and (4), the phases of the reflection coefficient  $\angle\Gamma_{co-pol}$  in these two cases differ in signs, i.e.  $\angle\Gamma_{co-pol} = -2\psi_{mn}$  for a RHCP incident wave while  $\angle\Gamma_{co-pol} = 2\psi_{mn}$  for a LHCP incident wave when the element is counter-clockwise rotated by an angle of  $\psi_{mn}$  [10].

From equation (1), the condition for the aperture distribution to be cophasal in the desired direction  $\vec{u}_0$  is

$$\phi_{mn} - k_0(|\vec{r}_{mn} - \vec{r}_f| + \vec{r}_{mn} \cdot \vec{u}_0) = 2k\pi, k = 0, 1, 2 \dots (5)$$

Here, the reflectarray is designed to radiate RHCP wave as its co-pol component. Thus, the co-pol component phase delay of the  $mn$ th element satisfies

$$-2\psi_{mn} - k_0(|\vec{r}_{mn} - \vec{r}_f| + \vec{r}_{mn} \cdot \vec{u}_0) = 2k\pi, k = 0, 1, 2 \dots (6)$$

Substituting (3) and (6) into (1), the reradiated RHCP field in the desired direction  $\vec{u}_0$  can be represented by

$$E_{RHCP}(\vec{u}_0) = \sum_{m=1}^{15} \sum_{n=1}^{15} A(\vec{r}_{mn} \cdot \vec{u}_0) \{ |\Gamma_{co-pol}| \cdot F_{RHCP}(\vec{r}_{mn} \cdot \vec{r}_f) \cdot e^{j2k\pi} + |\Gamma_{cross-pol}| \cdot F_{LHCP}(\vec{r}_{mn} \cdot \vec{r}_f) \cdot e^{j2k\pi} e^{j2\psi_{mn}} \} (7)$$

where  $F_{RHCP}$  and  $F_{LHCP}$  denote the pattern function of the feed horn in RHCP and LHCP, respectively. Similarly, the re-radiated LHCP field in the desired direction  $\vec{u}_0$  can be written as

$$E_{LHCP}(\vec{u}_0) = \sum_{m=1}^{15} \sum_{n=1}^{15} A(\vec{r}_{mn} \cdot \vec{u}_0) \{ |\Gamma_{co-pol}| \cdot F_{LHCP}(\vec{r}_{mn} \cdot \vec{r}_f) \cdot e^{j2k\pi} e^{j4\psi_{mn}} + |\Gamma_{cross-pol}| F_{RHCP}(\vec{r}_{mn} \cdot \vec{r}_f) e^{j2k\pi} e^{j2\psi_{mn}} \} (8)$$

For most of the elements,  $\psi_{mn} \neq n\pi$ , and it is evident that

$$\left| \sum_{m=1}^{15} \sum_{n=1}^{15} e^{j2\psi_{mn}} e^{j2k\pi} \right| < \left| \sum_{m=1}^{15} \sum_{n=1}^{15} e^{j2k\pi} \right|$$

$$\left| \sum_{m=1}^{15} \sum_{n=1}^{15} e^{j4\psi_{mn}} e^{j2k\pi} \right| < \left| \sum_{m=1}^{15} \sum_{n=1}^{15} e^{j2k\pi} \right| (9)$$

Since  $|F_{RHCP}(\vec{r}_{mn} \cdot \vec{r}_f)| > |F_{LHCP}(\vec{r}_{mn} \cdot \vec{r}_f)|$  in the main beam region when the feed horn is RHCP and  $|\Gamma_{co-pol}| > |\Gamma_{cross-pol}|$  across the element's bandwidth, it can be concluded from equations (7)-(9) that

1) To design an element rotated RHCP reflectarray with good performance in terms of antenna gain, the CP purity of the feed should be high. Otherwise, the incident LHCP field from the feed horn is dissipated according to equations (7) and (8), which wastes the incident LHCP power and results in a low gain and poor AE. Moreover, the reflected cross-pol component of the element should be low enough to keep the reflection of the incident RHCP field superposed in-phase. Otherwise, one part of the unwanted reflected field  $|\Gamma_{cross-pol}| F_{RHCP}(\vec{r}_{mn} \cdot \vec{r}_f) e^{j2k\pi} e^{j2\psi_{mn}}$  consumes the incident

RHCP power substantially and also results in a decreased gain.

2) It is possible to get an enhanced AR from the reflectarray even with a feed which has a large AR. Particularly considering a LP feed, the incident RHCP and LHCP power upon the aperture is the same. From equation (7), the reflected RHCP field can be greatly improved if  $|\Gamma_{co-pol}|$  is close to 1. Under the same condition, the reflected LHCP field is not superposed in-phase and thus is much smaller than the reflected RHCP field according to equation (8). Subsequently, the AR of the reflectarray is improved compared with the feed. However, the gain and AE of the reflectarray is reduced in this case since the incident LHCP power contributes little to the total gain as analyzed in conclusion (1).

To verify the above analysis, the proposed reflectarray is illuminated by two different feed horns, one is a wideband dual-CP horn with RHCP port excited and another one is an ideal RHCP horn which has infinite CP bandwidth and close to 0-dB AR. Besides, the aperture sizes of these two horns are all kept 50 mm×50 mm to give a similar gain and beamwidth at each frequency. When conducting the comparison, the two different feeds are placed at the same position to make the  $f/D$  unchanged. With these conditions, the spillover under these two cases is considered to be close to each other.

Fig. 8 shows the simulated AR of the proposed reflectarray with different feed horns. As shown, the AR bandwidth (AR<3 dB) of the dual-CP horn is from 6.7 GHz to 11.5 GHz and the AR bandwidth of the reflectarray using the dual-CP horn is from 7.2 GHz to 14.7 GHz. From 6.7 GHz to 7.2 GHz, the AR gets degraded from the horn to the array since the element reflection performance is rather bad in this frequency range. However, from 11.5 GHz to 14.7 GHz, the AR of the array gets improved although the dual-CP horn demonstrates poor CP purity in this frequency range. This mainly attributes to the function of the array as indicated in the above conclusion (2).

Fig. 9 shows the simulated gain of the proposed reflectarray with different feed horns. As shown, the gain of the reflectarray with dual-CP horn is smaller than the array with ideal horn from 11.5 GHz to 15 GHz. As analyzed in the aforementioned conclusion (1), the poor CP purity of the dual-CP horn in this frequency range results in the non-negligible LHCP incident field which contributes little to the gain of the array and yields a lower gain compared with the array using an ideal CP horn.

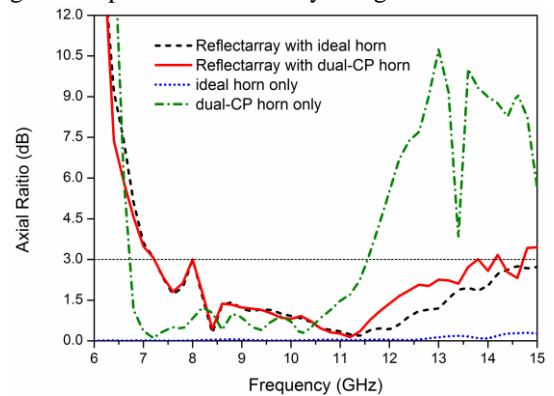


Fig. 8. Simulated AR of the proposed reflectarray with different feed horns.

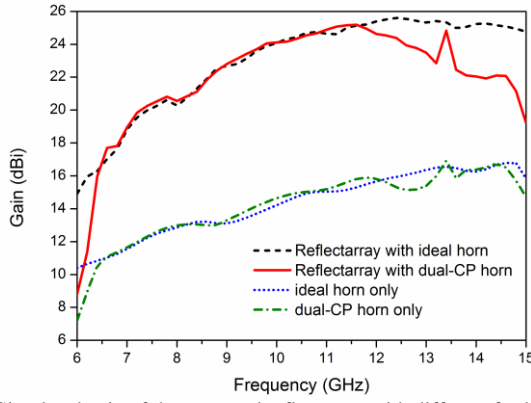


Fig. 9. Simulated gain of the proposed reflectarray with different feed horns.

### C. Effect of Differential Spatial Phase Delay

As indicated in Section III B, the proposed reflectarray achieves a 2:1 3-dB AR bandwidth. Due to this broad bandwidth, it is necessary to investigate the influence of the differential spatial phase delay to the gain bandwidth of the array, which increases as the working bandwidth increases. The bandwidth limitation of reflectarrays caused by the differential spatial phase delay is quantified for a broadside main beam and a prime focus feed in [25]. Here, equations are derived for more general cases, i.e. arbitrary feed position and arbitrary main beam direction to quantify the bandwidth limitation of reflectarrays due to the differential spatial phase delay.

Fig. 10 shows the geometry of a reflectarray with arbitrary feed position and arbitrary main beam direction. As shown, the diameter of the reflectarray is denoted by  $D$  while the focal length  $f = \sqrt{r^2 + h^2}$ . The feed horn is placed at an arbitrary position with an incident angle  $\theta_i$  to the aperture center  $O$  and the main beam direction is denoted by  $\theta_r$ .

Denoting the spatial phase delay from the feed to the aperture center  $O$  by  $PD_{FO}$  and the spatial phase delay from the feed to the edge of the aperture by  $PD_{FA}$  and  $PD_{FB}$ . As the main beam direction is  $\theta_r$ , the additional spatial phase delay introduced by the offset beam between the aperture center and the edge of the aperture is  $(k_0 D \cdot \sin \theta_r)/2$ . Therefore, the phase delay required by the aperture edge element A and B with respect to the aperture center  $O$  can be represented by  $PD_{AO}$  and  $PD_{BO}$ , which satisfy

$$\begin{aligned} PD_{AO} &= PD_{FA} - PD_{FO} - (k_0 D \cdot \sin \theta_r)/2 \\ PD_{BO} &= PD_{FB} - PD_{FO} + (k_0 D \cdot \sin \theta_r)/2 \end{aligned} \quad (10)$$

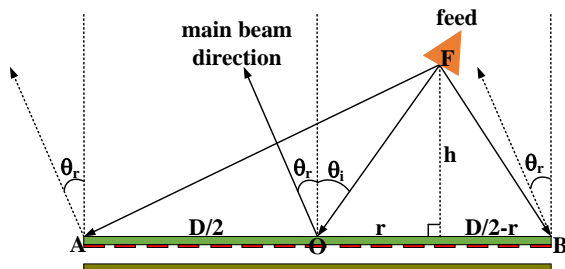


Fig. 10. Geometry of the reflectarray with arbitrary feed position and arbitrary main beam direction.

Let  $k_1$  and  $k_2$  be the wavenumbers at the design frequency  $f_1$  and operating frequency  $f_2$ , respectively. When the frequency shifts from the design frequency  $f_1$  to the operating frequency  $f_2$ , phase errors will be introduced to each element. Denote the phase error at the edge element A and B, relative to the phase at the center element, by  $PE_{AO}$  and  $PE_{BO}$ , which are

$$\begin{aligned} PE_{AO} &= (k_2 - k_1)R_A \\ PE_{BO} &= (k_2 - k_1)R_B \end{aligned} \quad (11)$$

where  $R_A = (\sqrt{(D/2 + r)^2 + h^2} - \sqrt{r^2 + h^2} - (D \cdot \sin \theta_r)/2)$  and  $R_B = (\sqrt{(D/2 - r)^2 + h^2} - \sqrt{r^2 + h^2} + (D \cdot \sin \theta_r)/2)$ , calculating from the geometry relationship shown in Fig. 10. According to [25], a reasonable criterion for evaluating the effect of this phase error is to evaluate the frequency shift for which this error equals  $180^\circ$  at the edge of the aperture. The intervening elements will incur less phase error, but out-of-phase radiation from edge elements A and B will begin to detract from the overall gain of the aperture. Let  $PE_{AO}$  and  $PE_{BO}$  equal to  $180^\circ$  and solve the frequency shift,  $\Delta f = f_2 - f_1$ , we can get:

$$\begin{aligned} \frac{\Delta f}{f_1} &= \frac{\lambda_1}{2R_A}, \text{ for } PE_{AO} = \pi \\ \frac{\Delta f}{f_1} &= \frac{\lambda_1}{2R_B}, \text{ for } PE_{BO} = \pi \end{aligned} \quad (12)$$

Substituting geometry dimensions  $D$ ,  $r$ ,  $h$  and  $\theta_r$  given in Fig. 6 (a) to equation (12), the frequency bandwidth  $2\Delta f/f_1$  for a circular aperture is roughly calculated to be 200% and 145.5% respectively for  $PE_{AO} = \pi$  and  $PE_{BO} = \pi$  (the design frequency  $f_1$  is 9 GHz). As this calculated bandwidth is wider than the element bandwidth, the bandwidth of the proposed reflectarray with  $15 \times 15$  elements is mainly determined by the bandwidth of elements and feed horn. But when the aperture size increases, the gain bandwidth will decrease. Specifically, it can be calculated from equation (12) that the aperture diameter  $D$  equals to 540 mm and 396 mm, respectively for  $PE_{AO} = \pi$  and  $PE_{BO} = \pi$  if the bandwidth  $2\Delta f/f_1$  is set to be 66% (the element bandwidth) and the  $f/D$  is kept unchanged. This indicates that the gain bandwidth of the proposed reflectarray will begin to decrease if the aperture diameter exceeds 396 mm (roughly equivalent to a 280 mm  $\times$  280 mm square array).

### D. Performance of S-Element-Based Reflectarrays with Larger Aperture Size

To analyze the performance of S-element-based reflectarrays with larger aperture size, another two arrays with elements of  $25 \times 25$  (300 mm  $\times$  300 mm) and  $45 \times 45$  (540 mm  $\times$  540 mm) are designed and simulated under the same  $f/D$  ratio as the  $15 \times 15$  element array presented above. Fig. 11 shows the simulated AR of the reflectarray with different aperture size. As shown, a 2:1 3-dB AR bandwidth can be maintained when the aperture size increases. Compared with the  $15 \times 15$  element array, the 3-dB AR bandwidth of the  $25 \times 25$  element array gets improved due to the fact that more elements are utilized, which makes the difference between the total reflected RHCP component and LHCP component larger than the case of  $15 \times 15$  element array.

When the array size increases to 540 mm×540 mm, the AR performance gets improved before 13 GHz and degrades after 13 GHz since the phase error caused by the spatial phase delay at the frequencies higher than 13 GHz is rather large (design frequency is 9GHz), which degrades the reflected RHCP component as well as the total antenna gain.

Fig. 12 shows the comparison of the simulated gain among the array with elements of 15×15, 25×25 and 45×45. As shown, the 3-dB gain bandwidth of the 15×15, 25×25 and 45×45 element array is 44.5%, 38.8% and 30.6%, respectively. Although the 3-dB gain bandwidth decreases as the aperture size increases, the proposed reflectarray with a large aperture size of 540 mm×540 mm ( $19.2\lambda \times 19.2\lambda$ ) still demonstrates much wider bandwidth than other reported CP reflectarrays with large aperture size [10, 11] in terms of both 3-dB AR bandwidth and 3-dB gain bandwidth.

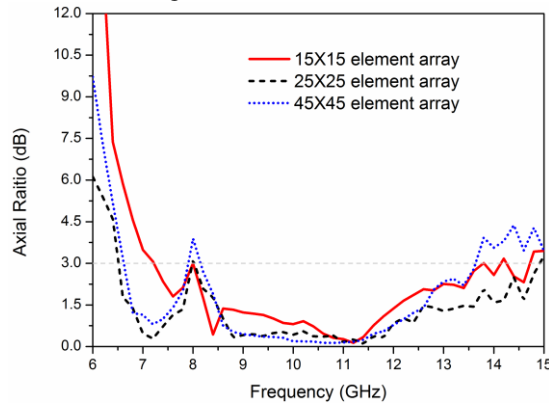


Fig. 11. Simulated AR of the reflectarray with elements of 15×15, 25×25 and 45×45.

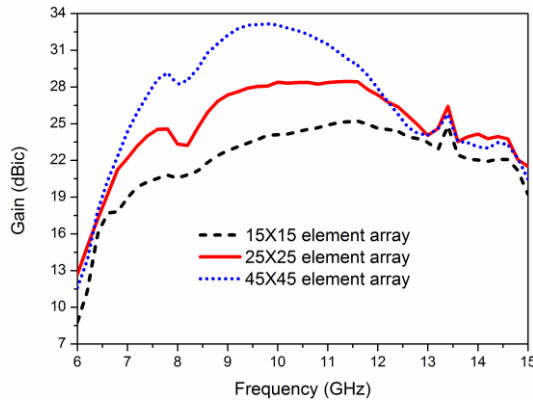


Fig. 12. Simulated gain of the reflectarray with elements of 15×15, 25×25 and 45×45.

#### IV. RESULTS AND DISCUSSIONS

##### A. Prototype and Reflection Coefficient

The fabricated prototype of the proposed antenna and the measurement setup in the anechoic chamber are shown in Fig. 13. As shown, the reflectarray is fed by a wideband dual-CP horn which uses a stepped-septum polarizer to simultaneously achieve  $TE_{10}$  and  $TE_{01}$  modes as well as a  $90^\circ$  phase shift between the two orthogonal electric field components [26].

The simulated and measured reflection coefficients of the proposed reflectarray are shown in Fig. 14. As shown, the array achieves a smaller than -10 dB reflection coefficient over a 2:1

frequency range. It is worthy pointing out that the  $S_{11}$  will degrade when a prime focus feed is utilized due to the blockage of the feed horn. To eliminate this phenomenon, an offset feed is chosen.

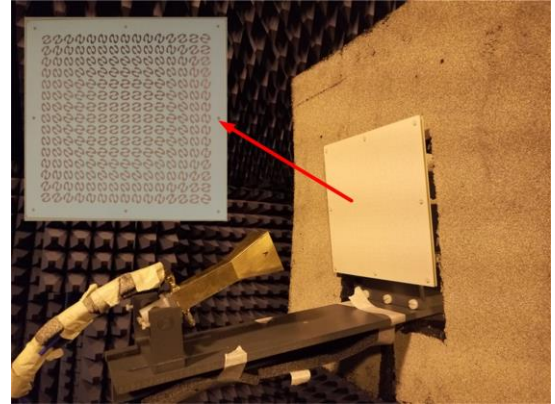


Fig. 13. The fabricated prototype and the measurement setup of the proposed antenna.

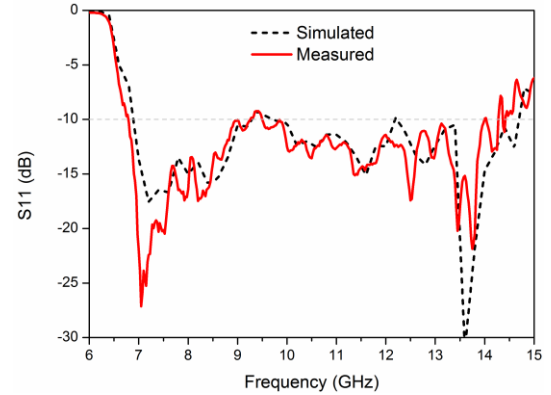


Fig. 14. Simulated and measured reflection coefficients of the reflectarray.

##### B. Axial Ratio

The simulated and measured AR of the proposed antenna are shown in Fig. 15. As shown, the measured 3-dB AR bandwidth is from 7.0 GHz to 14.3 GHz, corresponding to a fractional bandwidth of 68.5%.

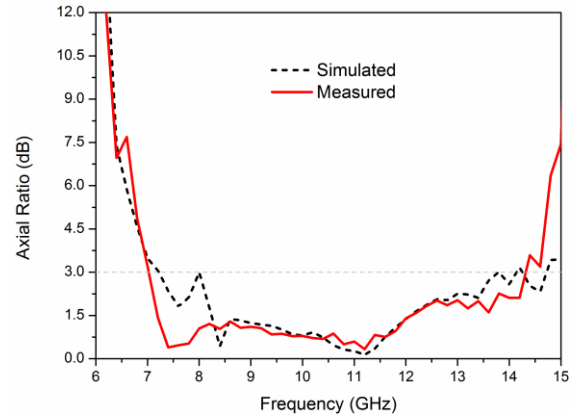


Fig. 15. Simulated and measured AR of the proposed antenna.

##### C. Realized Gain and Aperture Efficiency

Fig. 16 gives the simulated realized gain and measured gain of the proposed reflectarray. It is shown that the realized gain decreases rapidly when the frequency is lower than 7GHz. This is mainly caused by the drastic deterioration of the horn's



reflection coefficient when the frequency exceeds the working frequency range of the horn, as shown in Fig. 14. As shown in Fig. 16, the measured 3-dB gain variation bandwidth is from 8.6 GHz to 14 GHz (47.8%). The measured gain peaks at 11.4 GHz with a value of 25.25 dBic.

The aperture efficiency is also given by Fig. 16. The simulated AE is calculated based on the simulated realized gain while the measured AE is calculated by the measured gain. The difference between the results may stem from the fabrication errors of the horn and the array as well as the measurement errors. From the measured result, the reflectarray can achieve larger than 50% AE from 8.6 GHz to 12 GHz (33%) and larger than 30% AE from 7 GHz to 13.6 GHz (64%).

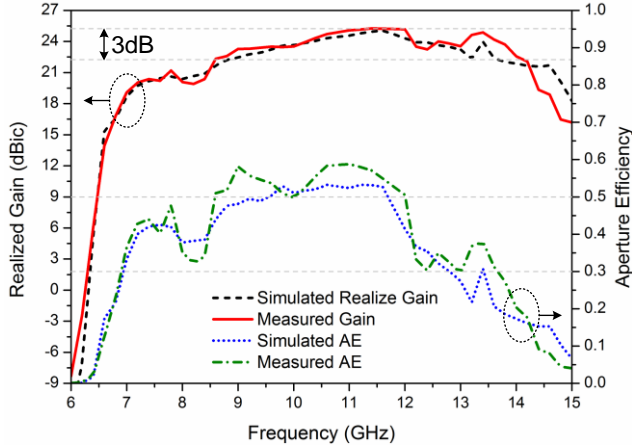


Fig. 16. Simulated and measured gain and efficiency of the proposed antenna.

#### D. Radiation Pattern

As aforementioned, the proposed reflectarray achieves a nearly 2:1 bandwidth in terms of impedance bandwidth, 3dB AR bandwidth and 30% AE bandwidth. Moreover, the proposed reflectarray can also maintain good radiation pattern performance such as undistorted radiation pattern shape, low sidelobe and low cross-pol component in a 2:1 bandwidth. To verify this, the radiation patterns at five different frequencies are shown in Fig. 17. The main plane 1 in Fig. 17 refers to the  $xoz$  plane as shown in Fig. 6 while the main plane 2 is the plane perpendicular to main plane 1 along the main beam direction.

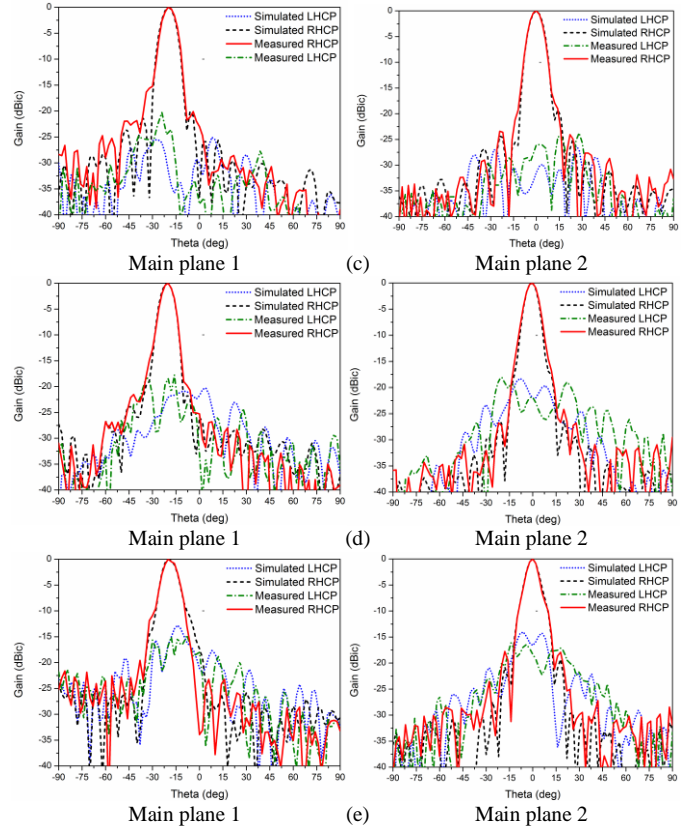
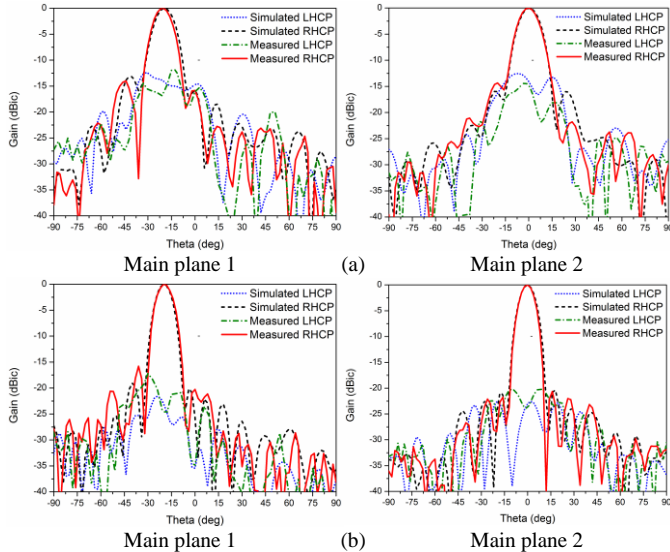


Fig. 17. Simulated and measured radiation patterns of the proposed antenna: (a) 7GHz, (b) 9GHz, (c) 10.6GHz, (d) 12GHz, (e) 14GHz.

As shown in Fig. 17, the measured radiation pattern agrees well with the simulated radiation pattern at each frequency. It is also observed from the results that the array maintains undistorted pencil-shaped beams, at least -15 dB side lobe and -15 dB cross-pol component from 7 GHz to 14 GHz.

#### E. Comparison with Other Wideband CP Reflectarrays

Due to the wideband characteristic of the novel S-shaped phasing element, the presented reflectarray achieves wide bandwidth in all aspects. To demonstrate its advantages more clearly, a comparison between the proposed design and other reported wideband CP reflectarrays is given by Table II. As shown in the table, the aperture size of the proposed design is comparable to the reference design [9, 19, 20] while it provides wider bandwidth (BW) in terms of 3-dB AR BW, 3-dB gain BW and radiation pattern BW. It is also noticed that the peak AE of the proposed reflectarray and [19] are much higher than the other designs with LP feed, which mainly attributes to the different element reflection performances under LP and CP incident waves. Moreover, the proposed reflectarray can maintain higher than 50% AE in a 33% bandwidth and larger than 30% AE in a 64% bandwidth, which also demonstrates its advantages over other designs.

#### V. CONCLUSION

A single layer wideband CP reflectarray using a novel S-shaped phasing element is presented. The proposed S-shaped element achieves low cross-pol reflection and very linear phase shift to the element rotation angle in a 2:1 bandwidth.



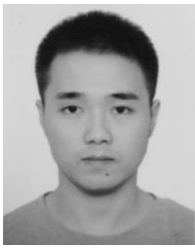
TABLE II  
COMPARISON WITH OTHER WIDEBAND CP REFLECTARRAYS

Ref. No.	Layers	Aperture Size (at center freq. )	f/D Ratio	Polarization of Feed	3-dB AR BW	Gain BW	AE BW	Peak Gain	Peak AE	Radiation Pattern BW
[9]	Single	$6.7\lambda \times 6.7\lambda$	0.84	LP	50%	1-dB gain 12.5%	-	24.4 dBic @ 12.5 GHz	46.3%	-
[17]	Single	$9\lambda \times 9\lambda$	1	LP	11%	1-dB gain 17%	-	25.8 dBic @ 9.8 GHz	39%	-
[18]	Dual	$4.2\lambda \times 4.2\lambda$	1	LP	28%	1-dB gain 20%	-	19.4 dBic @ 9.5 GHz	44%	-
[19]	Single	$6.5\lambda \times 6.5\lambda$	1	CP	43%	1-dB gain 31% 3-dB gain ~40%	-	~25 dBic @ 11.5 GHz	58.5%	-
[20]	Multi	Diameter: $7.8\lambda$	0.87	LP	40%	3-dB gain 40%	-	~25 dBic @ 11.5 GHz	~40%	40%
This work	Single	$6.4\lambda \times 6.4\lambda$	0.97	CP	68.5%	3-dB gain 47.8%	>50%: 33% >30%: 64%	25.2 dBic @ 11.6 GHz	60%	66.7%

Theoretical analysis indicates that the AR bandwidth of the CP reflectarray can be improved using element rotation method even with incident fields poor in CP purity. Moreover, the differential spatial phase delay is proved to have little effect to the bandwidth of small sized array but degrades the bandwidth of large sized array. The measurement results demonstrate that the proposed reflectarray has a 68.5% 3-dB AR bandwidth and a 47.8% 3-dB gain bandwidth. More importantly, the aperture efficiency of the proposed array is larger than 50% in a 33% bandwidth and larger than 30% in a 64% bandwidth. These excellent performances make the proposed reflectarray a good candidate for high-data-rate satellite communications.

## REFERENCES

- [1] J. Huang and J. A. Encinar, *Reflectarray Antennas*: John Wiley & Sons, 2007.
- [2] J. A. Encinar and J. A. Zornoza, "Broadband design of three-layer printed reflectarrays," *IEEE Trans. Antennas Propag.*, vol. 51, pp. 1662-1664, 2003.
- [3] J. A. Encinar, "Design of two-layer printed reflectarrays using patches of variable size," *IEEE Trans. Antennas Propag.*, vol. 49, pp. 1403-1410, 2001.
- [4] P.-Y. Qin, Y. J. Guo, and A. R. Weily, "Broadband Reflectarray Antenna Using Subwavelength Elements Based on Double Square Meander-Line Rings," *IEEE Trans. Antennas Propag.*, vol. 64, pp. 378-383, 2016.
- [5] Y. Mao, S. Xu, F. Yang, and A. Z. Elsherbeni, "A novel phase synthesis approach for wideband reflectarray design," *IEEE Trans. Antennas Propag.*, vol. 63, pp. 4189-4193, 2015.
- [6] E. Carrasco, J. A. Encinar, and M. Barba, "Bandwidth improvement in large reflectarrays by using true-time delay," *IEEE Trans. Antennas Propag.*, vol. 56, pp. 2496-2503, 2008.
- [7] S. Gao, Q. Luo, and F. Zhu, *Circularly polarized antennas*: John Wiley & Sons, 2013.
- [8] Y. Li, M. E. Bialkowski, and A. M. Abbosh, "Single layer reflectarray with circular rings and open-circuited stubs for wideband operation," *IEEE Trans. Antennas Propag.*, vol. 60, pp. 4183-4189, 2012.
- [9] G.-B. Wu, S.-W. Qu, S. Yang, and C. H. Chan, "Broadband, Single-Layer Dual Circularly Polarized Reflectarrays With Linearly Polarized Feed," *IEEE Trans. Antennas Propag.*, vol. 64, pp. 4235-4241, 2016.
- [10] J. Huang and R. J. Pogorzelski, "A Ka-band microstrip reflectarray with elements having variable rotation angles," *IEEE Trans. Antennas Propag.*, vol. 46, pp. 650-656, 1998.
- [11] A. Yu, F. Yang, A. Elsherbeni, J. Huang, and Y. Kim, "An offset-fed X-band reflectarray antenna using a modified element rotation technique," *IEEE Trans. Antennas Propag.*, vol. 60, pp. 1619-1624, 2012.
- [12] R. Deng, Y. Mao, S. Xu, and F. Yang, "A Single-Layer Dual-Band Circularly Polarized Reflectarray With High Aperture Efficiency," *IEEE Trans. Antennas Propag.*, vol. 63, pp. 3317-3320, 2015.
- [13] R. S. Malfajani and Z. Atlasbaf, "Design and implementation of a dual-band single layer reflectarray in X and K bands," *IEEE Trans. Antennas Propag.*, vol. 62, pp. 4425-4431, 2014.
- [14] C. Han, J. Huang, and K. Chang, "A high efficiency offset-fed X/Ka-dual-band reflectarray using thin membranes," *IEEE Trans. Antennas Propag.*, vol. 53, pp. 2792-2798, 2005.
- [15] T. Smith, U. Gothelf, O. S. Kim, and O. Breinbjerg, "An FSS-backed 20/30 GHz circularly polarized reflectarray for a shared aperture L-and Ka-band satellite communication antenna," *IEEE Trans. Antennas Propag.*, vol. 62, pp. 661-668, 2014.
- [16] W. A. Imbriale, S. Gao, and L. Boccia, *Space antenna handbook*: Wiley, 2012.
- [17] G. Zhao, Y.-C. Jiao, F. Zhang, and F.-S. Zhang, "A subwavelength element for broadband circularly polarized reflectarrays," *IEEE Antennas Wireless Propag. Lett.*, vol. 9, pp. 330-333, 2010.
- [18] L.-S. Ren, Y.-C. Jiao, F. Li, J.-J. Zhao, and G. Zhao, "A dual-layer T-shaped element for broadband circularly polarized reflectarray with linearly polarized feed," *IEEE Antennas Wireless Propag. Lett.*, vol. 10, pp. 407-410, 2011.
- [19] M.-Y. Zhao, G.-Q. Zhang, X. Lei, J.-M. Wu, and J.-Y. Shang, "Design of new single-layer multiple-resonance broadband circularly polarized reflectarrays," *IEEE Antennas Wireless Propag. Lett.*, vol. 12, pp. 356-359, 2013.
- [20] S. M. A. M. H. Abadi and N. Behdad, "Broadband True-Time-Delay Circularly-Polarized Reflectarray With Linearly-Polarized Feed," *IEEE Trans. Antennas Propag.*, vol. 64, pp. 4891-4896, 2016.
- [21] L. Zhang, S. Gao, Q. Luo, P. R. Young, W. Li, and Q. Li, "Inverted-S Antenna with Wideband Circular Polarization and Wide Axial Ratio Beamwidth," *IEEE Trans. Antennas Propag.*, vol. 65, pp. 1740 - 1748, 2017.
- [22] A. Mahmoud, A. A. Kishk, Z. Hao, and W. Hong, "Ka-band circularly polarized reflectarray: Using a double-layers cross slot," *IEEE Antennas Propag. Mag.*, vol. 58, pp. 60-68, 2016.
- [23] D. M. Pozar, S. D. Targonski, and H. Syrigos, "Design of millimeter wave microstrip reflectarrays," *IEEE Trans. Antennas Propag.*, vol. 45, pp. 287-296, 1997.
- [24] P. Nayeri, A. Z. Elsherbeni, and F. Yang, "Radiation Analysis Approaches for Reflectarray Antennas," *IEEE Antennas Propag. Mag.*, vol. 55, pp. 127-134, 2013.
- [25] D. M. Pozar, "Bandwidth of reflectarrays," *Electron. Lett.*, vol. 39, pp. 1490-1491, 2003.
- [26] J. Bornemann and V. A. Labay, "Ridge waveguide polarizer with finite and stepped-thickness septum," *IEEE Trans. Microw. Theory Tech.*, vol. 43, pp. 1782-1787, 1995.



**Long Zhang** received the B.S. and M.S. degrees in electrical engineering from Huazhong University of Science and Technology (HUST), Wuhan, China, in 2009 and 2012, respectively; and the Ph.D. degree in electronic engineering from the University of Kent, Canterbury, U.K, in 2017.

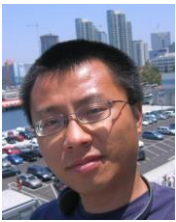
He is currently an Assistant Professor with the College of Information Engineering, Shenzhen University, China. His research interests include circularly polarized antennas, smart antennas, reconfigurable antennas, mobile terminal antennas, phased arrays, tightly coupled arrays, and reflectarrays.



**Steven Gao** (M'01–SM'16) received the Ph.D. degree in microwave engineering from Shanghai University, Shanghai, China, in 1999.

He is a Professor and Chair in RF and microwave engineering with the University of Kent, Canterbury, U.K. He co-authored two books including *Space Antenna Handbook* (Wiley, 2012) and *Circularly Polarized Antennas* (IEEE-Wiley, 2014), published more than 250 papers, and holds several patents in smart antennas and RF. His research interests include smart antennas, phased arrays, satellite antennas,

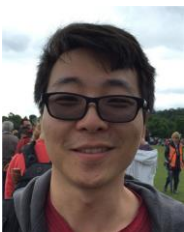
RF/microwave/mm-wave/THz circuits, satellite communications, UWB radars, synthetic-aperture radars, and mobile communications.



**Qi Luo** (S'08–M'12) received the M.Sc degree in data communications from the University of Sheffield, Sheffield, U.K., in 2006; and the Ph.D. degree in electrical engineering from the University of Porto, Porto, Portugal, in 2012.

From 2012 to 2013, he was a Research Fellow with the Surrey Space Centre, Guildford, U.K. Currently, he is a Research Associate with the School of Engineering and Digital Arts, University of Kent, Canterbury, U.K. His research interests include smart antennas,

circularly polarized antennas, reflectarray, multiband microstrip antennas, and electrically small antenna design.



**Wenting Li** received the B.S. degree in Electronic Information Engineering and the M.S. degree in Electromagnetic Field and Microwave Technology from Northwestern Polytechnical University (NPU), Xi'an, China, in 2011 and 2014, respectively. He is currently pursuing the Ph.D. degree at the University of Kent, Canterbury, U.K.

His research interests include reflectarray antennas, reconfigurable antennas, circularly polarized antennas and multi-beam antennas.



**Yejun He** (SM'09) received the Ph.D. degree in information and communication engineering from Huazhong University of Science and Technology (HUST), Wuhan, China, in 2005.

From 2005 to 2006, he was a Research Associate with the Department of Electronic and Information Engineering, Hong Kong Polytechnic University, Hong Kong. From 2006 to 2007, he was a Research Associate with the Department of Electronic Engineering, Faculty of Engineering, Chinese University of Hong Kong, Hong Kong. In 2012, he was

a Visiting Professor with the Department of Electrical and Computer Engineering, University of Waterloo, Waterloo, ON, Canada. From 2013 to 2015, he was an Advanced Visiting Scholar (Visiting Professor) with the School of Electrical and Computer Engineering, Georgia Institute of Technology, Atlanta, GA, USA. Since 2011, he has been a Full Professor with the College of Information Engineering, Shenzhen University, Shenzhen, China, where He is the Director of Guangdong Engineering Research Center of Base Station Antennas and Propagation, and the Director of Shenzhen Key Laboratory of Antennas and Propagation, Shenzhen, China. He has authored or

coauthored more than 100 research papers, books (chapters) and holds 13 patents. His research interests include channel coding and modulation, 4G/5G wireless mobile communication, space-time processing, antennas and RF.

Dr. He is serving as Associate Editor of IEEE Access, Security and Communication Networks. He has served as a Reviewer for various journals such as the IEEE TRANSACTIONS ON VEHICULAR TECHNOLOGY, the IEEE TRANSACTIONS ON COMMUNICATIONS, the IEEE TRANSACTIONS ON WIRELESS COMMUNICATIONS, the IEEE TRANSACTIONS ON INDUSTRIAL ELECTRONICS, the IEEE WIRELESS COMMUNICATIONS, the IEEE COMMUNICATIONS LETTERS, IEEE JOURNAL ON SELECTED AREAS IN COMMUNICATIONS, International Journal of Communication Systems, Wireless Communications and Mobile Computing, and Wireless Personal Communications. He has also served as a Technical Program Committee Member or a Session Chair for various conferences, including the IEEE Global Telecommunications Conference (GLOBECOM), the IEEE International Conference on Communications (ICC), the IEEE Wireless Communication Networking Conference (WCNC), and the IEEE Vehicular Technology Conference(VTC). He is the Principal Investigator for over 20 current or finished research projects including NSFC of China, the Integration Project of Production Teaching and Research by Guangdong Province and Ministry of Education as well as the Science and Technology Program of Shenzhen City. He is a Fellow of IET.



**Qingxia Li** (M'08) received the B.S., M.S., and Ph.D. degrees in electrical engineering from Huazhong University of Science and Technology (HUST), Wuhan, China, in 1987, 1990, and 1999, respectively.

He is currently a Professor in Science and Technology on Multi-Spectral Information Processing Laboratory, School of Electronic Information and Communications, HUST. His current research interests include microwave remote sensing and deep space exploration, electromagnetic theory and application,

antenna array and signal processing.